Supplementary Figures

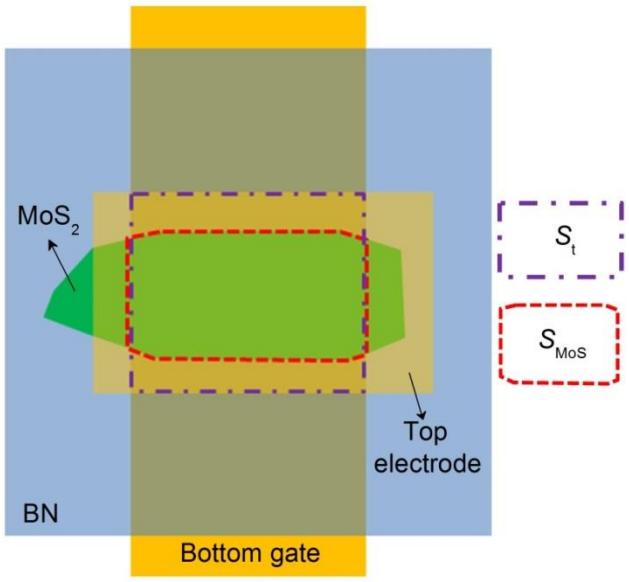

Supplementary Figure 1 | Analysis of the device geometry. S_t is the total effective capacitance area enclosed by the purple dash-dot line. S_{MoS} is the effective area of MoS_2 enclosed by the red dashed line.

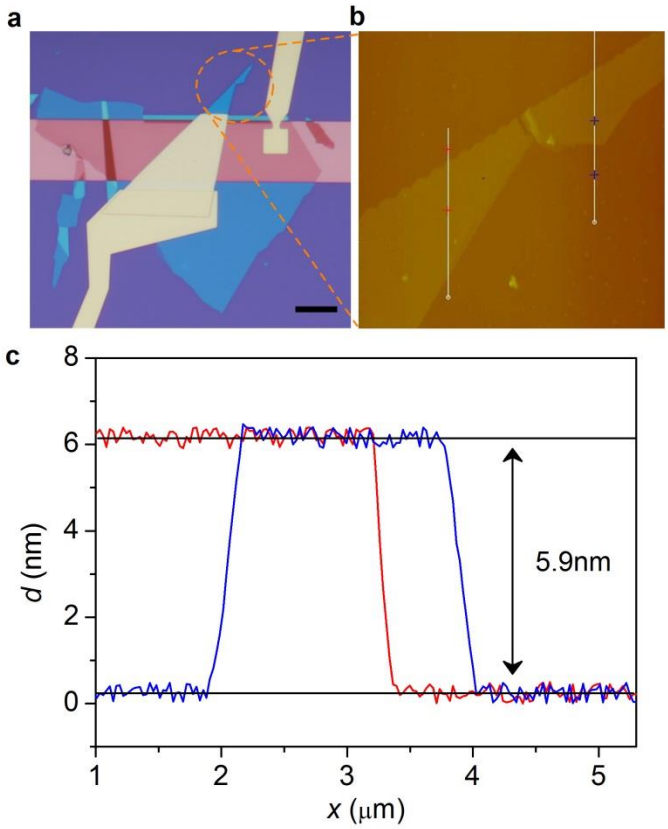

Supplementary Figure 2 | Determination of the thickness of MoS_2 by AFM. (**a**) Optical image of the 5.9nm-thick MoS_2 sample shown in the main text. (**b**,**c**) AFM image (**b**) and the thickness (**c**) of the MoS_2 sample.

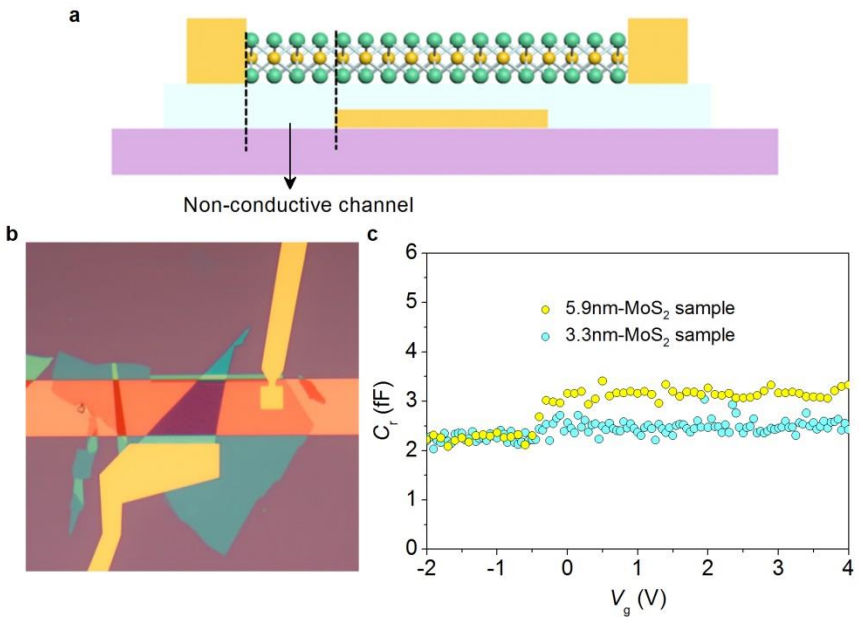

Supplementary Figure 3 | Determination of the residual capacitance C_r. (**a**) Schematic image of the MoS_2 sample without overlapping between the top electrode and bottom gate. (**b**) Optical image of the 5.9 nm-MoS_2 sample before covering the top electrode. (**c**) Residual capacitance determined in the 5.9 nm-MoS_2 sample along with a 3.3 nm-MoS_2 sample. It is three-order smaller than the capacitance of MoS_2 devices.

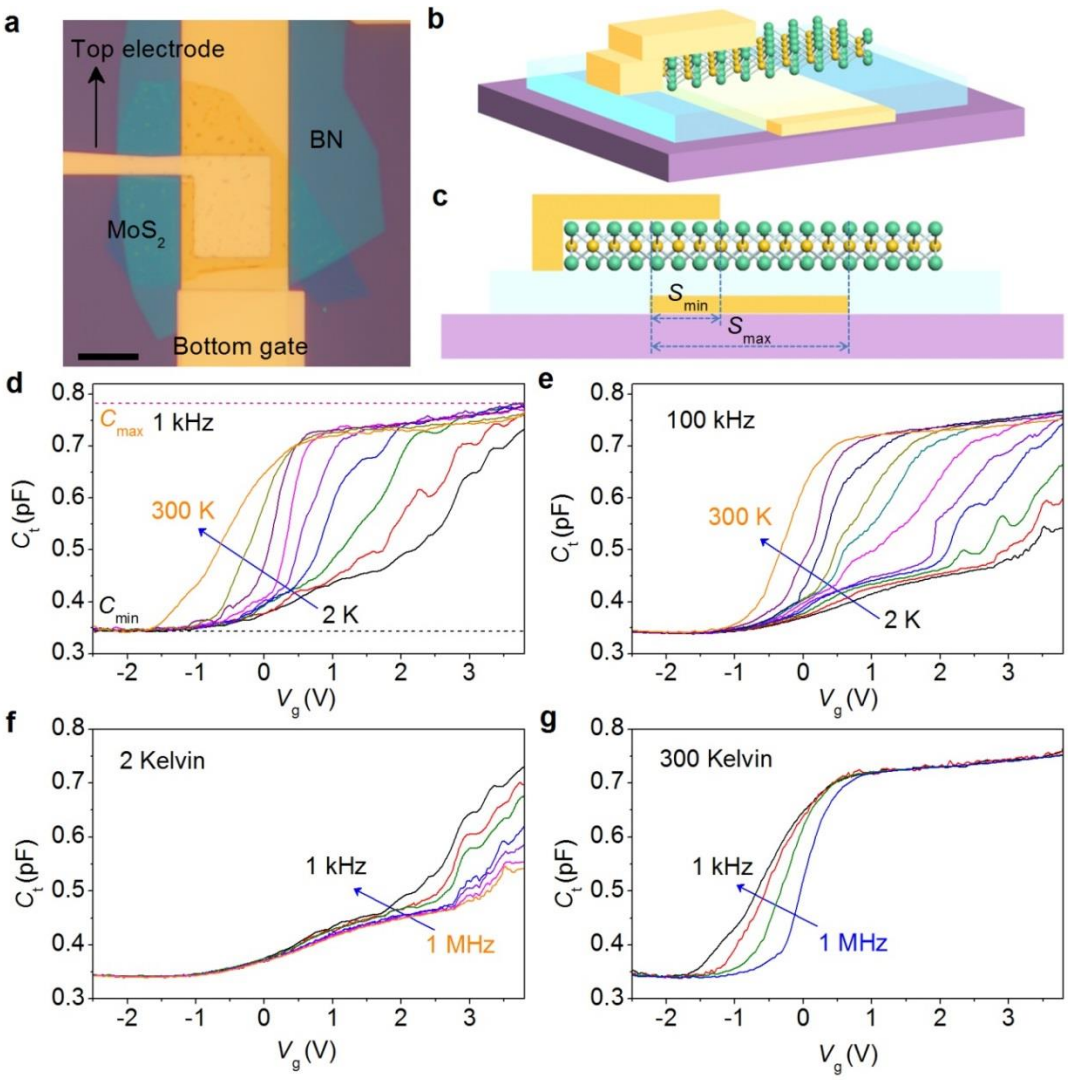

Supplementary Figure 4 | Capacitance characteristics for a monolayer MoS_2 in MIS-FET geometry. (**a-c**) Optical (**a**) and schematic images (**b**,**c**) of the partially-covered top electrode geometry for capacitance measurements. Scale bar is 10 μm. (**d**,**e**) C_t at excitation frequency 1 kHz (**d**) and 100 kHz (**e**) for different temperatures. (**f**,**g**) C_t at temperature 2 K (**f**) and 300 K (**g**) for different excitation frequencies.

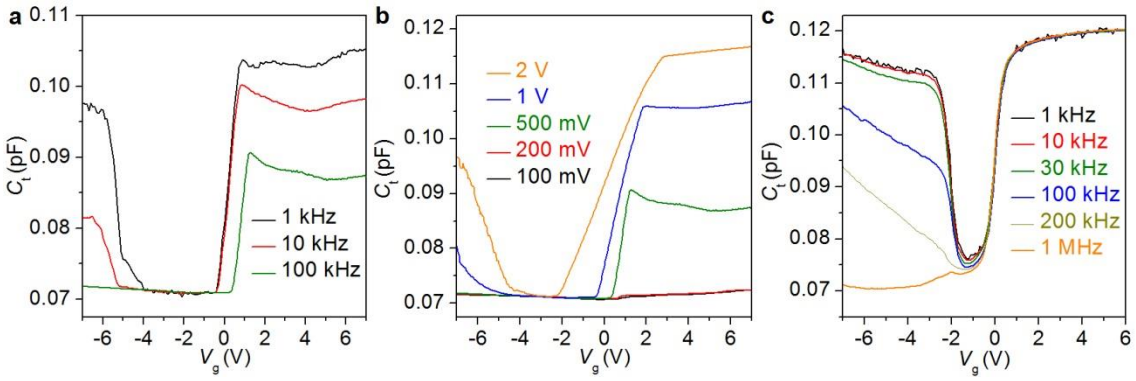

Supplementary Figure 5 | MoS_2 capacitance with Cr/Au electrodes. (**a**) Measured capacitance C_t at 2 K with an excitation voltage 500 mV for different frequencies. (**b**) C_t at 2K with an excitation frequency 100 kHz at different excitation voltages. (**c**) C_t at 300 K with an excitation voltage 200 mV for different frequencies.

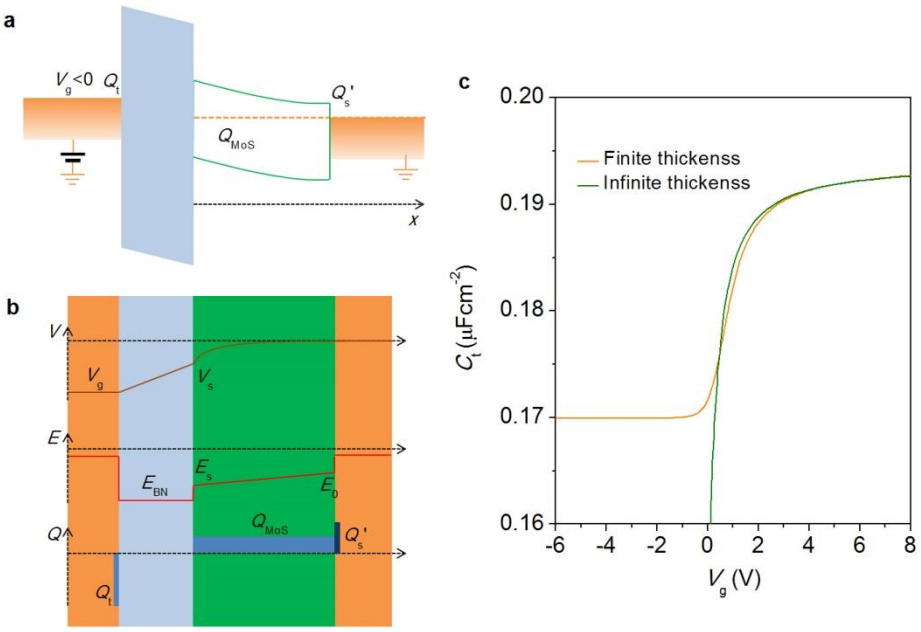

Supplementary Figure 6 | Modeling of capacitance devices. (**a**) Schematic band diagram at the depletion region. (**b**) Schematic image of potentials, electric fields, and charge distributions in the capacitance device. (**c**) Simulated total capacitance C_t as a function of gate voltage V_g with a finite thickness $d_{eff} = 5.9\text{nm}$ (orange line) and an infinite thickness (green line).

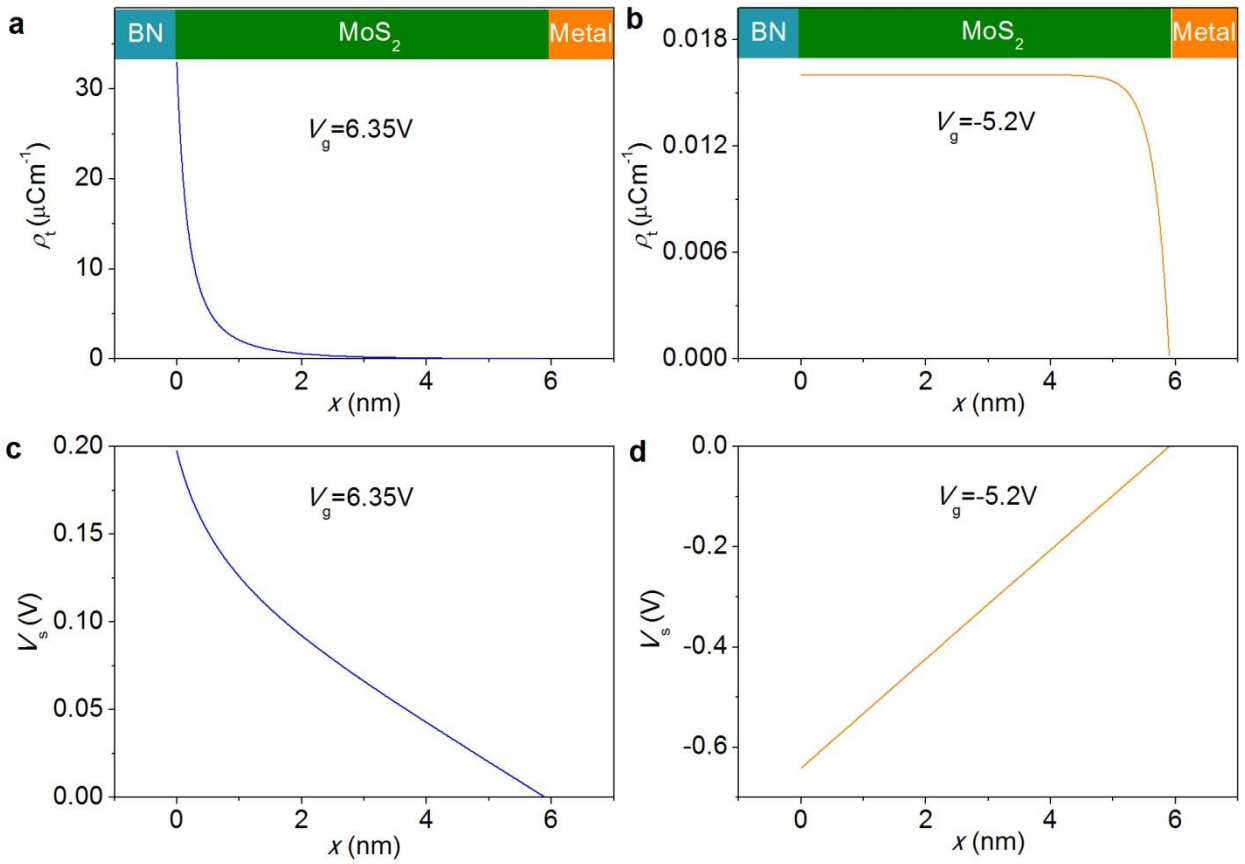

Supplementary Figure 7 | Charge and potential distributions in MoS_2. (**a**,**c**) Charge (**a**) and potential (**c**) distributions in the accumulation region with a gate voltage $V_g = 6.35\text{V}$ in the MoS_2 capacitance device. (**b**,**d**) Charge (**b**) and potential (**d**) distributions in the depletion region with a gate voltage $V_g = -5.2\text{V}$.

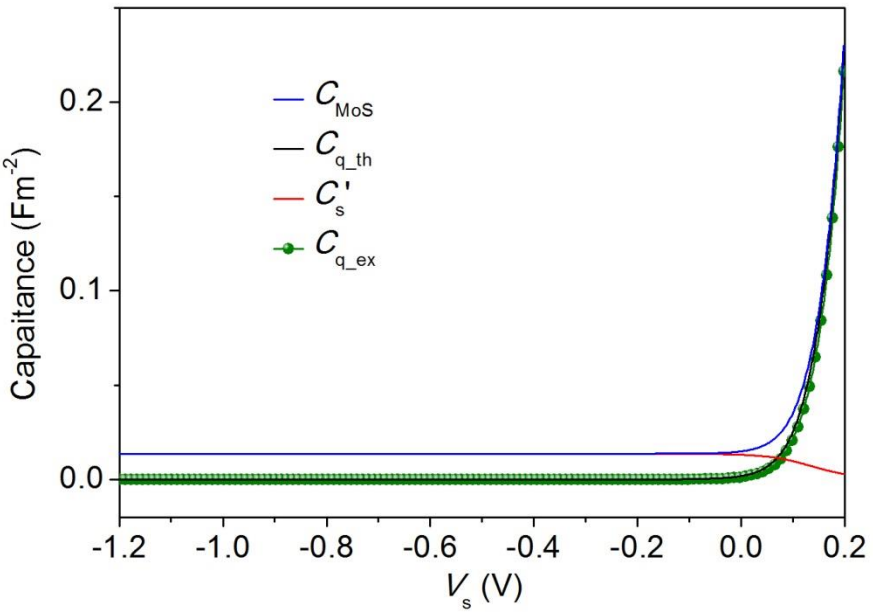

Supplementary Figure 8 | Extraction of the quantum capacitance of MoS_2. Simulated results of C_{MoS}, C_s' and C_{q_th} without adopting any approximation. C_{q_ex} is a good approximation of C_{q_th}.

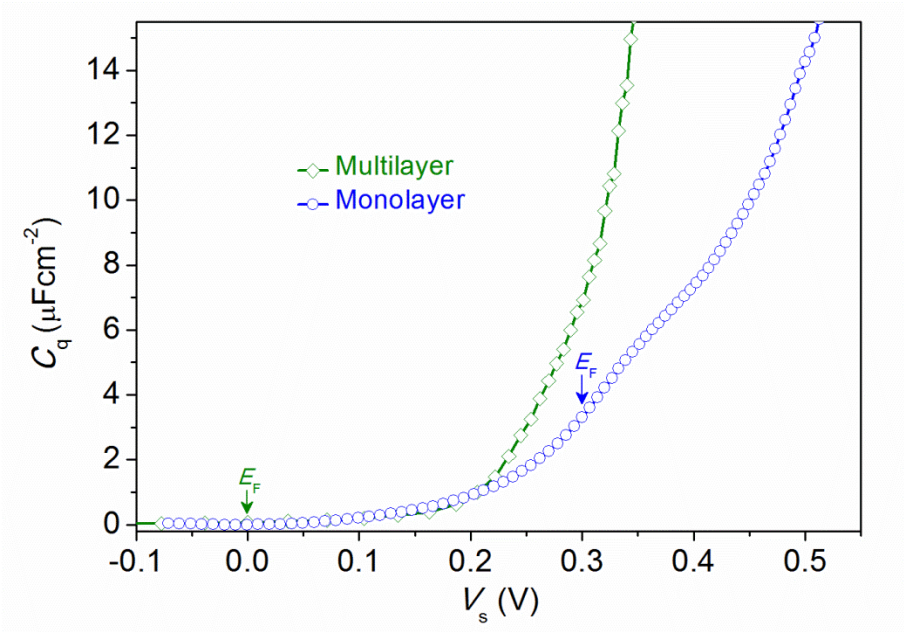

Supplementary Figure 9 | Quantum capacitance in MoS_2 samples. Quantum capacitance as a function of surface potential in multilayer and monolayer MoS_2. E_F denotes the Fermi energy position when the gate voltage $V_g = 0$.

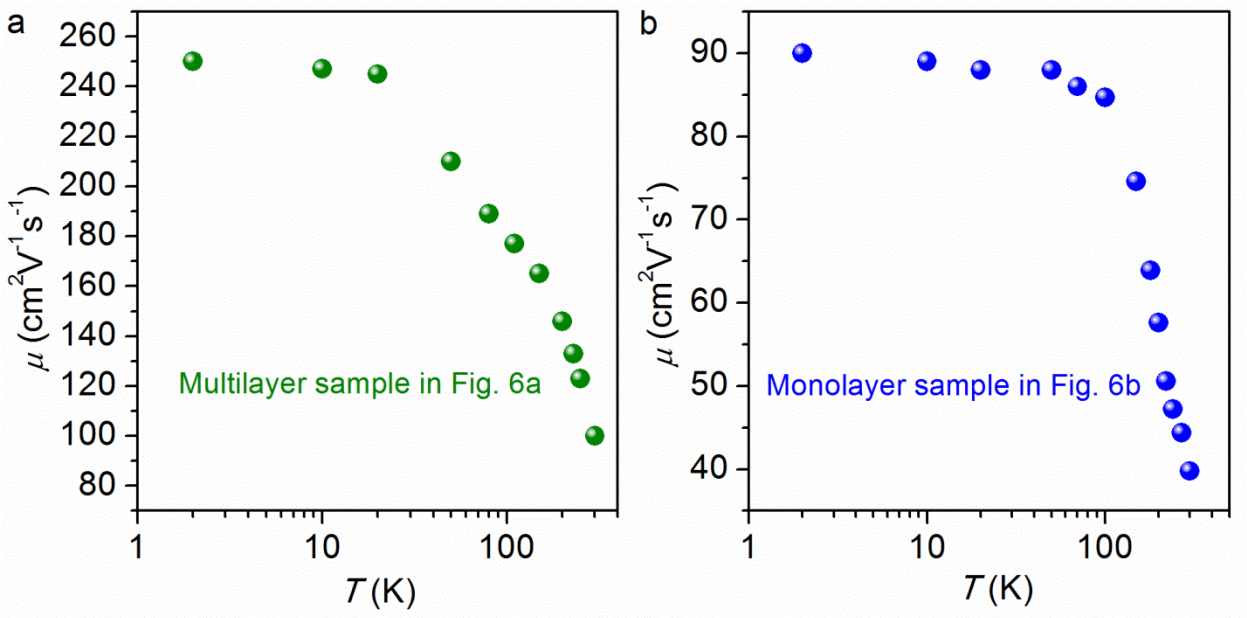

Supplementary Figure 10 | Mobility of MoS_2 samples. (**a**) Mobility of the multilayer MoS_2 at n~8.5x10^{12} cm^{-2}. (**b**) Mobility of the monolayer MoS_2 at n~1.3x10^{13} cm^{-2}.

Supplementary Notes

Supplementary Note 1

Extracting the parallel capacitance C_p

To accurately determine the charge trap densities, dielectric constant and quantum capacitance of MoS_2, the parallel capacitance C_p shown in Fig. 1c has to be determined first. C_p contains two terms: the residual capacitance C_r originating from the measurement setup (the measurement of C_r will be introduced in next section which is negligible compared to C_{ex}) and the parallel capacitance C_{ex} originating from the extra area of the top electrode, as shown in Supplementary Fig. 1.

S_t is the total effective capacitance area enclosed by the purple dash-dot line. S_{MoS} is the effective area of MoS_2 enclosed by the red dashed line. The extra area of the top electrode is $S_{ex} = S_t - S_{MoS}$. The actual capacitance $C_t' = C_t + C_{ex} + C_r$, where C_t is the capacitance shown in the main text which excludes the extra capacitance $C_{ex} = S_{ex} \cdot \frac{\varepsilon_{BN}}{d_{BN}}$ and C_r. Then capacitance C_t equals to $C_t = (C_{MoS}^{-1} + C_g^{-1})^{-1}$ which corresponds to area S_{MoS}.

To determine C_{ex}, we only need to know the capacitance of BN per unit area, which can be simply obtained through measuring the reference capacitor shown in Fig. 1a in the main text. We have measured the thicknesses of MoS_2 and BN sheets by atomic force microscopy (AFM) in order to determine the dielectric constant of MoS_2 (Supplementary Fig. 2). The thickness of BN is 14 nm for 5.9 nm-MoS_2 device, 6.0 nm for monolayer-MoS_2 device, 14.9 nm for trilayer-MoS_2 device, and 13.5 nm for 12 nm-MoS_2 device as shown in the main text. The extracted dielectric constant of BN is around 3.1, consistent with previous results[1].

Supplementary Note 2

Determining the residual capacitance C_r

The residual capacitance C_r is accurately determined by a simple method shown in Supplementary Fig. 3. In the device structure without any overlap between the top electrode and bottom gate (Supplementary Fig. 3a), there is a non-conductive channel in MoS_2 which cannot be tuned by the bottom gate. Charges from electrodes are blocked from reaching the MoS_2 area above the bottom gate. Then, the measured capacitance should be the residual capacitance C_r induced by the measurement setup. The optical image of the 5.9 nm-MoS_2 sample before covering the top electrode is shown in Supplementary Fig. 3b. The measured capacitance along with a 3.3 nm-MoS_2 sample is plotted in Supplementary Fig. 3c. We find that the capacitance values of C_r are in the order of ~fF, which is about 3-order smaller than the MoS_2 capacitances. Hence, the residual capacitance C_r is ignored in our calculations.

Supplementary Note 3

Capacitance measurements on MoS_2-based FET structures

Based on standard field-effect transistor (FET) structures, the top electrode is partially covered on MoS_2 as shown in Supplementary Fig. 4a-c (a monolayer MoS_2 sample). S_{max} represents the overlapping area between the bottom gate and MoS_2, and S_{min} represents the overlapping area between the top electrode and the bottom gate. In the partially-covered top electrode structure, $S_{min} < S_{max}$. Supplementary Fig. 4d-g show the capacitance results from a monolayer MoS_2 sample partially covered by a Ti/Au electrode. Under a negative bias, MoS_2 is in the depleted

state, and the measured capacitance can be described by $C_{\min} = S_{\min} \cdot (\frac{d_{BN}}{\varepsilon_{BN}} + \frac{d_{MoS}}{\varepsilon_{MoS}})^{-1}$. With increasing the gate voltage, electrons start to accumulate at the surface of MoS_2 and the channel becomes conductive. Then, the measured capacitance approaches $C_{\max} = S_{\max} \cdot \frac{\varepsilon_{BN}}{d_{BN}}$. The ratio of $C_{\max}$ and $C_{\min}$ for this sample is $C_{\max} / C_{\min} \approx S_{\max} / S_{\min} = 2.2$. This is because the term $\frac{\varepsilon_{MoS}}{d_{MoS}}$ only contributes about one twentieth of the capacitance $C_{\min}$, which is negligible in comparison to the capacitance increase caused by the increase of conducting area (from $S_{\min}$ to $S_{\max}$) of MoS_2.

The capacitance measured from the partially-covered MoS_2 devices largely depends on temperatures and frequencies as shown in Supplementary Fig. 4d-g. The capacitance increases with decreasing excitation frequencies. This is consistent with previously reported results measured at 300 K[2]. The frequency-dependent behavior of the partially-covered devices becomes serious at low temperatures (Supplementary Fig. 4f). MoS_2 sheets are normally not fully charged at low temperatures and higher frequencies. This is attributed to the charge trapping effect or the huge lateral resistance of MoS_2 near the band edge. Hence, some intrinsic characteristics of MoS_2 are smeared, especially at cryogenic temperatures.

Supplementary Note 4

Capacitance measurements on the MoS_2 device with Cr/Au top electrodes.

The work function of Cr (~4.5 eV) is larger than that of Ti (~4.3eV). Hence, Cr is much closer to the valence band of MoS_2, and a smaller relaxation time of holes should be observed. In the MoS_2 sample coated with a Cr/Au electrode (Supplementary Fig. 5a), the formation of the

inversion layer is observed at 2 K where the contribution of thermal effects can be neglected. As confirmed by the capacitance results measured at different excitation voltages (Supplementary Fig. 5b), leakage current (to the electrode contacts) plays an important role. Large excitation voltages can contribute significantly to the formation of holes. As the work function of Cr is about 0.2 eV higher than the electron affinity of MoS_2 (~4.3 eV), the relaxation of electrons is also subjected to the Schottky barrier (Supplementary Fig. 5a,b) which shows frequency- and temperature-dependent behavior in capacitance measurements. At 300 K, the relaxation time of holes is much shorter (~5 μs) than that at low temperatures, while the capacitance measured at the electron side is almost frequency-independent.

Supplementary Note 5

Modeling capacitance devices and extracting the quantum capacitance C_q of thin MoS_2 flakes

Here, we applied the Poisson equation to investigate our capacitance devices quasi-quantitatively and consider a simplified one-dimensional model[3] as shown in Supplementary Fig. 6a and b:

$$\frac{d^2V}{dx^2} = -\frac{e(n_D^{+} - n - p_A^{-} + p)}{\varepsilon_{MoS}} \quad (1)$$

where V is the potential of MoS_2 at position x. n_D^{+} and p_A^{-} are the densities of electron and hole donors respectively. n and p represent the electron and hole carrier densities. Assuming n_0 and p_0 are the equilibrium densities of electrons and holes respectively (at $V = 0$), we have $n = n_0 \exp(\frac{eV}{kT})$ and $p = p_0 \exp(-\frac{eV}{kT})$, where k is the Boltzmann constant. When $V = 0$, the

charge neutrality condition applies, and we have $n_{\mathrm{D}}^{+} - p_{\mathrm{A}}^{-} = n_0 - p_0$. Here, we only focus on the depletion and accumulation regions of MoS_2 devices where $n_0 >> p_0$. Then the Poisson equation can be simplified as:

$$\frac{d^2V}{dx^2} = \frac{en_0}{\varepsilon_{\mathrm{MoS}}}[\exp(\frac{eV}{kT}) - 1] \tag{2}$$

As the electric field in MoS_2 is described by $E = -\frac{dV}{dx}$, the integral of Eq. (2) yields:

$$E = \sqrt{E_0^{\,2} + \frac{2k^2T^2}{e^2L_{\mathrm{D}}^{\,2}}[\exp(\frac{eV}{kT}) - \frac{eV}{kT} - 1]} \tag{3}$$

where $L_{\mathrm{D}} = \sqrt{\frac{\varepsilon_{\mathrm{MoS}}kT}{e^2n_0}}$ is the Debye length. E_0 is the electric field at position $x = d_{\mathrm{MoS}}$ (the interface between MoS_2 and top electrode shown in Supplementary Fig. 6a,b). E_0 is a non-zero value and mainly determined by the gate voltage V_{g} because of the finite thickness of MoS_2. E_0 can be obtained through the constraint condition $\int_0^{V_{\mathrm{s}}} \frac{dV}{E} = d_{\mathrm{MoS}}$, where V_{s} is the surface potential of MoS_2. As a result, any additional charges $Q_{\mathrm{s}}' = \varepsilon_{\mathrm{MoS}}E_0$ will be accumulated at the interface between the top electrode and MoS_2 (Supplementary Fig. 6a,b). The total charges induced in the device can be described by $Q_{\mathrm{t}} = \varepsilon_{\mathrm{MoS}}E_{\mathrm{s}} = Q_{\mathrm{MoS}} + Q_{\mathrm{s}}'$, where E_{s} is the surface electric field of MoS_2, and Q_{MoS} is the surface charges in MoS_2.

The simulating parameters for Supplementary Fig. 6, 7, and 8 are: $\varepsilon_{\mathrm{MoS}} = 8.6$, $d_{\mathrm{MoS}} = 5.9\mathrm{nm}$, $\varepsilon_{\mathrm{BN}} = 3$, $d_{\mathrm{BN}} = 13.5\mathrm{nm}$ and doping density $n_{\mathrm{D}}^{+} = 10^{17}\,\mathrm{cm}^{-2}$. The simulated total capacitance $C_{\mathrm{t}} = \frac{dQ_{\mathrm{t}}}{dV_{\mathrm{g}}}$ as a function of V_{g} is shown in Supplementary Fig. 6c. Compared to C_{t} of MoS_2 with

an infinite thickness, C_t with a finite value of d_{MoS} approaches a constant value $(\frac{d_{MoS}}{\varepsilon_{MoS}}+\frac{d_{BN}}{\varepsilon_{BN}})^{-1}$ in the depletion region, consistent with the experimental observations shown in the main text. The simulations for charge and potential distributions in MoS_2 are shown in Supplementary Fig. 7. In the accumulation region, most of charges are distributed in the first several layers of MoS_2. While in the depletion region, the charge density is small (mainly originated from the density of electron donors n_D^+). As a result, the charge distribution is almost constant in MoS_2. This analysis also supports that the effective thickness d_{eff} decreases with increasing the gate voltage.

The capacitance of MoS_2 $C_{MoS}=\frac{dQ_t}{dV_s}$ can be written as $C_{MoS}=C_q+C_s'$, where $C_q=\frac{dQ_{MoS}}{dV_s}$ is the quantum capacitance of MoS_2 and $C_s'=\frac{dQ_s'}{dV_s}$ originates from the charges induced at the interface between the top electrode and MoS_2. C_{MoS} can be obtained from the serial connection relationship $C_t=(C_{MoS}^{-1}+C_g^{-1})^{-1}$. However, it is difficult to directly determine C_s' as discussed below.

Here, we present an approximate method to satisfactorily extract the quantum capacitance (C_q) of MoS_2, supported by theoretical calculations. The accurate C_{MoS}, C_s' and C_{q_th}, without adopting any approximation, are theoretically simulated and shown in Supplementary Fig. 8. In the depletion region, both C_s' and C_{MoS} approaches a constant value C_{s0}. With increasing the gate voltage, C_s' decreases due to the stronger screening effect of accumulated charges at the surface of MoS_2. While, C_{q_th} increases rapidly. The quantum capacitance of MoS_2 can be approximately written in the form of $C_{q\_ex}=C_{MoS}-C_{s0}$ instead of $C_{q\_th}=C_{MoS}-C_s'$ with a good accuracy as shown in Supplementary Fig. 8. In the depletion region, all charges form at the

interface between the top electrode and MoS_2. Then, we have $C_{MoS} = C_s'$, and $C_{q\_th} = C_{q\_ex} = 0$. The approximation is accurate in the depletion region. In the accumulation region, $C_s' < C_{s0}$ and there exists deviation between the approximation value C_{q_ex} and the accurate value C_{q_th}. In this case, surface charges dominate the total induced charges in the device and thus $C_{q\_th} >> C_s'$. Obviously, the deviation is small compared to the value of C_{q_th}. Overall, $C_{q\_ex} = C_{MoS} - C_{s0}$ is a good approximation to the accurate value of C_{q_th}.

Supplementary Note 6

Quantum capacitance in monolayer and multilayer MoS_2

The extracted quantum capacitance of monolayer and 12nm-multilayer MoS_2 is shown in Supplementary Fig. 9. The measured quantum capacitance of monolayer MoS_2 is smaller than the value in multilayer MoS_2.

Supplementary Note 7

Transport properties of monolayer and multilayer MoS_2

The mobility of multilayer and monolayer MoS_2 samples (in Fig. 6) at different temperatures is shown in Supplementary Fig. 10. The mobility of the monolayer and multilayer MoS_2 sample is around $90 cm^2V^{-1}s^{-1}$ and $250 cm^2V^{-1}s^{-1}$ respectively at 2 K.

Supplementary References

1. Dean, C. R. *et al.* Boron nitride substrates for high-quality graphene electronics. *Nat Nanotech.* **5**, 722-726 (2010).

2. Zhu, W. J. *et al.* Electronic transport and device prospects of monolayer molybdenum disulphide grown by chemical vapour deposition. *Nat Commun.* **5**, 3087 (2014).

3. Kingston, R. H. &Neustadter, S. F. Calculation of the space charge, electric field, and free carrier concentration at the surface of a semiconductor. *J. Appl. Phys.* **26**, 718 (1955).